Revised manuscript version-3 submitted to Cement and Concrete Research

Rietveld Quantitative Phase Analyses of SRM 2686a: a Standard Portland Clinker

M. García-Maté[a], G. Álvarez-Pinazo[a], L. León-Reina[b], A. G. De la Torre[c], M. A. G. Aranda[c,d,*]

[a] X-Ray Data Services S.L., Edificio de Institutos Universitarios, Oficina 11C, C/ Severo Ochoa 4, Parque Tecnológico de Andalucía, 29590 Málaga, Spain.

[b] Servicios Centrales de Apoyo a la Investigación, Universidad de Málaga, 29071, Málaga, Spain.

[c] Departamento de Química Inorgánica, Universidad de Málaga, Campus Teatinos S/N. 29071, Málaga, Spain.

[d] ALBA Synchrotron, Carrer de la Llum 2-26. 08290 Cerdanyola del Vallès, Barcelona, Spain.

* email: g_aranda@uma.es or migarcia@cell.es

KEYWORDS:

Mineralogical content, synchrotron radiation, powder diffraction

ABSTRACT:

SRM 2686a is a NIST reference Portland clinker with reported mineralogical analysis from powder diffraction and electron microscopy. This sample is used in ASTM C1365 test method for Rietveld quantitative phase analysis validation procedure. Here, we have analysed SRM 2686a by using three state-of-the-art powder diffraction configurations: i) strictly monochromatic CuKα_1 radiation in flat reflection geometry; ii) strictly monochromatic MoKα_1 radiation in flat transmission geometry; and iii) synchrotron radiation in rotating capillary transmission geometry. The silicate and aluminate enriched residues have also been studied by CuKα_1 powder diffraction. All the powder patterns were analysed by Rietveld method with the best available protocols. The results indicate that belite in SRM 2686a is composed of two polymorphs (β- and α'_H-) that must be included in the analyses. The use of a unique phase for describing belite (β-polymorph) and improper peak shape modelling could explain the problems found for implementing ASTM C1365 in some cement manufacturing plants. Furthermore,

all the patterns are deposited as open data access at Zenodo, so interested laboratories can analyse these data to verify their protocols.

1. Introduction.

Building materials, such as Portland cements (PCs), are multiphase systems of worldwide importance and quantitative knowledge of their mineralogical composition is necessary to predict their performances [1]. In fact, the hydraulic properties of mortars and concretes mainly depend on the cement mineralogical composition (and its texture and water-cement ratio) [2-4].

X-ray powder diffraction (XRPD) data analysed by using the Rietveld method may yield the crystalline mineralogical composition of the sample [5,6]. This approach is becoming the most widely used technique to determine the mineralogical composition in the building material field [7-9]. Rietveld Quantitative Phase Analysis (RQPA) using laboratory-XRPD was firstly applied to a Portland clinker in 1993 [10]. Eight years later, RQPA of Portland cement was obtained by using synchrotron-XRPD [11]. Nowadays, XRPD is routinely used in the cement industry for bulk mineralogical phase analysis [12].

There are reported guidelines for carrying out Rietveld studies [13] and two Round Robin studies on RQPA of PCs gave valuable recommendations for performing analyses as accurate as possible [14,15]. The determination of the possible amorphous content in PCs has also being researched by two different methodologies, external and internal standard methods [16,17]. The application of RQPA to PCs, although of widespread use [7,8,18,19], is not straightforward for the following main reasons [8,19,20]: *_sample-related* i) phases can crystallize as several polymorphs that must be identified a priori; ii) the atomic impurities inside each phase are not known and their scale factors are usually computed for ideal/stoichiometric phases; *_technique-related* iii) each phase has its own mass absorption coefficient (and average particle size) which could cause microabsorption problem; *_refinement-related* iv) there are many phases, usually more than five, which increases the diffraction peak overlapping and so the

correlations in the fits; v) some phases, for instance alite, calcite or gypsum, show preferred orientation, increasing the errors; vi) for minor content phases, the peak shape modelling is critical; and vii) the diffraction peak broadening for some phases may be anisotropic that must be properly modelled. Furthermore, the small irradiated volume (~ 2 mm^3) for CuKα (the most used radiation) may lead to poor particle statistics even after sample rotation. For accurate results, and assuming that the samples are rotated, the particle sizes must be smaller than approximately 10 μm.

Having a standard reference clinker sample is very important twofold: i) to test the experimental data collection, equipment and strategy; and ii) to verify that used Rietveld protocol is adequate. In this context, the National Institute of Standards and Technology (NIST) offers the reference material, SRM 2686a, which is a Portland clinker with a reported overall mineralogical analysis from XRPD and electron microscopy [21]. Furthermore, the Compositional Analysis subcommittee of American Society for Testing and Materials (ASTM) C01.23 developed a test method, ASTM C1365 [22], entitled 'Determination of the Proportion of Phases in Portland Cement and Portland-Cement Clinker Using X-Ray Powder Diffraction Analysis'. This test method considers the use of XRPD data analysed by the Rietveld method and it is being used for cement industries to self-verify their RQPA procedures.

In the course of our research in RQPA of cementitious materials, and due to our interactions with manufacturing cement plants, we have been aware of cement plants having problems to validate their RQPA methodologies by using the ASTM C1365 test method. In this procedure, the maximum and minimum ranges for the different crystalline components of SRM 2686a are stated, following the average mineralogical analysis provided by NIST. Therefore, the aim of this study is to carry out a thorough RQPA study of NIST SRM 2686a sample with the best possible data and Rietveld protocol(s). In order to do so, several XRPD patterns were collected for SRM 2686a using different radiations: i) strictly monochromatic $CuK\alpha_1$ radiation in reflection geometry (flat rotating sample); ii) strictly monochromatic $MoK\alpha_1$ radiation in transmission geometry (flat rotating sample); and iii) synchrotron radiation in transmission geometry (rotating capillary). The powder patterns were analysed

by Rietveld method. Furthermore, silicate and aluminate enriched residues have been produced using selective dissolution and they were also analysed by the Rietveld method. The results indicate that the reported NIST analysis for belite comprises two polymorphs that must be included in the Rietveld control file in order to successfully implement ASTM C1365.

2. Materials and Methods.

2.1. Material.

SRM 2686a sample, directly purchased from NIST, was used in this study. Table 1 shows its mineralogical analysis reported by NIST [21]. The maximum variation allowed by ASTM C1365 test method for each phase [22] is also included in the table. The clinker was ground by a McCrone micronising mill for 10 min with isopropanol, then it was vacuum filtered and dried at 40ºC during 24 hours in a stove.

2.2. Selective dissolution methods.

The SRM 2686a sample was chemically treated using the selective dissolution methods in order to enrich the silicate and aluminate fractions. The milled SRM 2686a sample was passed through a 65 μm sieve. A solution of sucrose in aqueous potassium hydroxide was used to obtain the silicate enriched residue, which mainly contains belite and alite [23,24]. A salicylic acid in methanol solution was employed to obtain the aluminate enriched residue, which mainly contains aluminates, ferrite and periclase, by stirring 1 g of clinker during 3 hours and left motionless for l8 hours [23]. Successive filtering, washing with methanol and drying at 75ºC in a stove were performed before XRD data collection.

2.2. Analytical techniques.

2.2.1. Laboratory X-ray powder diffraction.

Three laboratory XRPD patterns were recorded in reflection geometry (θ/2θ) on a X'Pert MPD PRO (PANalytical B.V., The Netherlands) diffractometer equipped with a Ge (111) primary monochromator

which resulted in strictly monochromatic CuKα_1 radiation, λ=1.54059 Å. The X-ray tube worked at 45 kV and 40 mA. The optics configuration was a 0.5º fixed divergence slit, a 1º fixed incident anti-scatter slit, a 0.5º fixed diffracted anti-scatter slit and X'Celerator RTMS (real-time multiple strip) detector, working in the scanning mode with the maximum active length. The samples were back-loaded employing a PANalytical powder sample preparation kit designed to minimise preferred orientation. Using these conditions, the sample was measured between 5-70º (2θ) with a step size of 0.0167º and with a total measurement time of 5 hours and 16 minutes by spinning the sample at 10 rpm. This powder pattern is hereafter named Cu-LXRPD.

A second type of laboratory XRPD powder pattern was collected in flat transmission geometry (θ/θ), with the sample placed between two Kapton foils [25], in constant irradiated volume mode, on a D8 ADVANCE DaVinci (Bruker AXS, Germany) diffractometer. The diffractometer has a Molybdenum X-ray tube and the use of a Johansson Ge (111) primary monochromator renders a strictly monochromatic MoKα_1 radiation, λ=0.7093 Å. The X-ray tube worked at 50 kV and 50 mA. The optics configuration was a 0.1º fixed divergence slit, and a 9 mm fixed diffracted anti-scatter slit. The energy-dispersive linear detector LYNXEYE XE 500 μm, optimized for high energy radiation, was used with the maximum opening angle. Using these conditions the samples were measured between 3-35º (2θ) with a step size of 0.020º and with a total measurement time of 10 hours and 27 minutes by spinning the sample at 10 rpm. This powder pattern is hereafter named Mo-LXRPD. In both diffractometers, there are two containers with silica gel and KOH pellets to maintain the H_2O and CO_2 contents as lows as possible.

2.2.2. Transmission synchrotron X-ray powder diffraction.

The synchrotron powder pattern was collected in Debye-Scherrer (transmission) mode using the X-ray powder diffraction station of ALBA Synchrotron Light Source [26]. The wavelength, λ= 0.82543(5) Å, was selected with a double-crystal Si (111) monochromator and determined from a Si640d NIST standard (a=5.43123 Å). The data were recorded using the MYTHEN detector system. The sample was

loaded in glass capillary of 0.5 mm of diameter and rotated during data collection to improve diffracting particle statistics. To attain a very good signal-to-noise ratio over the angular range 1-35º (2θ) and to improve the accuracy of the diffraction data, the acquisition time was 20 min per dataset at three different positions along the capillary. The three datasets were summed-up to produce the final pattern which is hereafter named SXRPD.

2.2.3. Data analysis.

The powder patterns were analysed by the Rietveld method as implemented in the TOPAS software package v5 (Bruker AXS, Germany). The fundamental parameter approach was used to analyse Cu-LXRPD and Mo-LXRPD patterns. Table S1, deposited as supplementary information, gives the instrument parameters used to perform the refinements. The SXRPD instrumental profile shape function was empirically modelled by measuring NAC sample [27], in exactly the same experimental conditions. To do so, additional convolutions approach [28] was employed and the appropriated values were refined to model the contribution to instrumental profile shape of the axial divergence (Circles), detector slit (Hat), crystal size (Lorentzian) and strains (Gaussian), see Table S1. Finally, these values were kept fixed to analyse the SXRPD pattern.

The backgrounds were modelled as a Chebychev function with orders 6, 8 and 20 for Cu-LXRPD, Mo-LXRPD and SXRPD patterns, respectively. The scale factors were refined for all phases. Lattice parameters were refined for the phases with contents larger than 2.0 wt%. Sample displacement, or zero-shift for capillaries, was also refined for each pattern. Alite showed preferred orientation which was corrected by using March-Dollase algorithm [29]. A Double-Voigt approach [30] was used to model microstructure effects. The Lorentzian contribution of crystal size to peak profile was refined for all the phases except for sulfates, for these phases the value was kept fixed to the value 200 nm. Moreover, alite and C_4AF showed anisotropic line-shape broadening, likely due to solid solution, which was modelled by refining the Gaussian contribution of strains to peak profile.

2.2.4. Particle size distribution.

The particle size distribution of the milled clinker was measured by laser diffraction in isopropanol suspension using a Malvern MasterSizer S (UK) instrument. The powder was previously dispersed in isopropanol in test tubes using an ultrasonic bath.

3. Results and discussion.

Figure 1 displays the particle size distribution of SRM 2686a after sample preparation for the powder diffraction analyses. $D_{v,50}$ and $D_{v,90}$ values were 4.4 and 14.1 μm, respectively. The average results for the analyses of the silicate and aluminate enriched residues are reported in Table 2, while the direct results of the triplicates have been deposited as supplementary information in Tables S2 (silicate enriched residue) and S3 (aluminate enriched residue). Figure 2 shows the Rietveld plots for one of the replicates for both residues together with the similar plot for the SRM 2686a clinker. The key result extracted from these analyses was to determine the presence of α'_H-C_2S, see inset in Figure 2b. From the analyses of the silicate enriched residue powder patterns, it was also determined the absence of γ-C_2S. Furthermore, the modelling of the peak shape parameters can be better carried out in the patterns collected for the residues as there are less phases and therefore less correlation between parameters. For the aluminate enriched residues, the unit cell parameters of cubic-C_3A and ortho-C_3A were refined. These values converged to a=15.236 Å for cubic-C_3A; a=10.850 Å, b=10.822 Å and c=15.095 Å for ortho-C_3A and they were kept fixed for the Rietveld analyses of the clinkers where their contents were much smaller, see Tables 2 and 3. The used ICSD codes for all the phases are reported in Table 3.

Figure 3 displays a selected range of the Rietveld plots for the three types of patterns. It is evident from the visual inspection of Figure 3 that SXRPD has the sharpest diffraction peaks (minimum peak overlapping), as expected. This is mainly observable in the degree of splitting of the alite peaks. However, it is also clear that the diffraction peaks of the aluminate phases (tricalcium aluminate and ferrite) are much broader than those from alite, which was also expected. Aluminates crystallize during cooling and preserving smaller mean crystallite sizes (and likely less ordered). Furthermore, Figure 3

also shows that Mo-LXRPD pattern has the broadest diffraction peaks and so diffraction peak overlapping is more pronounced for this dataset. However, this drawback could be compensated with the larger irradiation volume [20] which enhances particle statistics when compared to datasets collected with Cu-radiation in flat reflection geometry.

Alite shows preferred orientation along the [-1 0 1] direction of the substructure of M_3 polymorph. This is evident in Figure 3 as the peak located close to 32.2º (2θ), for Cu-LXRPD, has higher relative intensity as data were collected in reflection for a flat sample. The same peak located close to 14.7º (2θ), for Mo-LXRPD, has lower relative intensity as data were collected in transmission for a flat sample. These effects were modelled and corrected through the March-Dollase algorithm [29]. The refined values were approximately 0.94 for the Cu-LXRPD patterns, see Table 4, and 1.053(5) and 1.014(2) for the Mo-LXRPD and SXRPD patterns, respectively.

The RQPA results for SRM 2686a derived from the three patterns are reported in Table 3, the average values from the three replicates for the Cu-LXRPD data are included here. The direct RQPA results for each replicate are deposited as supplementary information in Table S4. It must be highlighted that we have carried out three types of analyses for having a comprehensive approach but the synchrotron RQPA (SRQPA) results are likely the most accurate as the diffraction data have the narrowest peak width for alite, belite and periclase, leading to the lowest overlapping. The diffraction peaks are intrinsically broad for aluminate and sulfate phases. Table 3 also gives the reported data (overall phase contents in two cases: belites, aluminates and sulfates) by NIST for the sake of comparison. Moreover, the RQPA results when only β-belite is included in the control file are also reported. In this case, the total belite content is systematically lower, of the order of 15 wt%. The modelling of the peak shape, mainly for the low content phases, is key to obtain reproducible phase contents. Therefore, Table 4 reports all the peak shape parameters used for the fits of the Cu-LXRPD patterns. Furthermore, it is

deduced from the values reported in Table 3 that the results from synchrotron powder diffraction are very similar to those derived from laboratory data with strictly monochromatic radiations.

The comparison of the phase contents for the three types of analyses of this work and the data reported by NIST, see Table 3, shows that the agreement is very good. The novelty of this work is to report the contents of the different polymorphs and the protocol to properly model the peak shapes. With this important consideration, all the measured phase contents are within the ASTM C1365 limits.

4. Conclusions

The analyses reported here show that NIST SRM 2686a clinker has two polymorphs for belite. The α'_H-polymorph, and not only β-belite, is necessary to obtain phase contents within the ASTM C1365 limits, with a proper modelling of the shape of the diffraction peaks. The results given here indicate that the reported NIST analysis overestimates belite content which may explain problems found for implementing ASTM C 1365 in some cement manufacturing plants. This protocol may be useful for laboratories of cement factories to verify their procedures. All the patterns analysed here can be accessed on Zenodo at https://doi.org/10.5281/zenodo.1318500, and used under the Creative Commons Attribution license.

Acknowledgments: This work has been supported by Spanish MINECO through BIA2014-57658-C2-2-R, which is co-funded by FEDER, and BIA2014-57658-C2-1-R. We also thank ALBA synchrotron for providing beam time at BL04-MSPD beamline.

REFERENCES

[1] H.F.W. Taylor, "Cement Chemistry", 2nd Ed. Thomas Telford, UK, London, 1997.
[2] D.P. Bentz, A review of early-age properties of cement-based materials, Cem. Concr. Res. 38 (2008) 196–204.
[3] J. Skibsted, C. Hall, Characterization of cement minerals, cements and their reaction products at the atomic and nano scale, Cem. Concr. Res. 38 (2008) 205–255.
[4] K.L. Scrivener, A. Nonat, Hydration of cementitious materials, present and future, Cem. Concr. Res. 41 (2011) 651–665.
[5] I.C. Madsen, N.V.Y. Scarlett, L.M.D. Cranswick, T. Lwin, Outcomes of the International Union

of Crystallography Commission on powder diffraction round robin on quantitative phase analysis: samples 1a to 1h, J. Appl. Crystallogr. 34 (2001) 409–426.
[6] N.V.Y. Scarlett, I.C. Madsen, L.M.D. Cranswick, T. Lwin, E. Groleau, G. Stephenson, M. Aylmore, N. Agron-Olshina, Outcomes of the International Union of Crystallography Commission on Powder Diffraction Round Robin on Quantitative Phase Analysis: samples 2, 3 and 4, synthetic bauxite, natural granodiorite and pharmaceuticals, J. Appl. Crystallogr. 35 (2002) 383–400.
[7] G. Le Saout, V. Kocaba, V., K. Scrivener, Application of the Rietveld method to the analysis of anhydrous cements. Cem. Concr. Res. 41 (2011) 133-148.
[8] M.A.G. Aranda, A.G. De la Torre, L. Leon-Reina, Rietveld quantitative phase analysis of OPC clinkers, cements and hydration products, Rev. Mineral. Geochem. 74 (2012) 169–209.
[9] P. Stutzman, Direct Determination of Phases in Portland Cements by Quantitative X-Ray Powder Diffraction, NIST Technical Note 1692, (2011) 59 pages.
[10] J.C. Taylor, L.P. Aldridge, Full-profile Rietveld quantitative XRD analysis of Portland cement: Standard XRD profiles for the major phase tricalcium silicate (C3S: 3CaO.SiO2). Powder Diffraction 8 (1993) 138–144.
[11] A.G. De la Torre, A. Cabeza, A. Calvente, S. Bruque, M.A.G. Aranda, Full Phase Analysis of Portland Clinker by Penetrating Synchrotron Powder Diffraction. Anal. Chem. 73 (2001) 151–156
[12] R. Meier, J. Anderson, S. Verryn, Industrial X-ray Diffraction Analysis of Building Materials, Rev. Mineral. Geochem. 74 (2012) 147–165.
[13] L.B. McCusker, R.B. Von Dreele, D.E. Cox, D. Louer, P. Scardi, Rietveld Refinement Guidelines. J. Appl. Cryst. 32 (1999) 36–50.
[14] P. Stutzman, Powder diffraction analysis of hydraulic cements: ASTM Rietveld round-robin results on precision, Powder Diffraction 20 (2005) 97–100.
[15] L. León-Reina, A.G. De la Torre, J.M. Porras-Vázquez, M. Cruz, L.M. Ordonez, X. Alcobé, F. Gispert-Guirado, A. Larranaga-Varga, M. Paul, T. Fuellmann, R. Schmidt, M.A.G. Aranda, Round robin on Rietveld quantitative phase analysis of Portland cements, J. Appl. Crystallogr. 42 (2009) 906–916.
[16] D. Jansen, Ch. Stabler, F. Goetz-Neunhoeffer, S. Dittrich, J. Neubauer, Does Ordinary Portland Cement contain amorphous phase? A quantitative study using an external standard method, Powder Diffraction 26 (2011) 31–38.
[17] R. Snellings, A. Bazzoni, K. Scrivener, The existence of amorphous phase in Portland cements: Physical factors affecting Rietveld quantitative phase analysis, Cem. Concr. Res. 59 (2014) 139–146.
[18] A.G. De la Torre, I. Santacruz, L. León-Reina, A. Cuesta, M.A.G. Aranda, Diffraction and crystallography applied to anhydrous cements" pp 3-29 in 'Cementitious Materials. Composition, Properties, Application' Editor: Herbert Pöllmann. De Gruyter Publishing, 2017. ISBN: 978-3110473735
[19] M.A.G. Aranda, A.G. De la Torre, L. Leon-Reina, Powder diffraction characterisation of cements, in 'International Tables for Crystallography, Volume H, Powder Diffraction', in press. Eds. C. Gilmore, J. Kaduk, H. Schenk (2018). ISBN: 978-1-118-41628-0.
[20] L. León-Reina, M. García-Maté, G. Álvarez-Pinazo, I. Santacruz, O. Vallcorba, A.G. De la Torre, M.A.G. Aranda, Accuracy in Rietveld quantitative phase analysis: a comparative study of strictly monochromatic Mo and Cu radiations, J. Appl. Cryst. 49 (2016) 722–735.
[21] Certificate of Analysis. Standard Reference Material 2686a. Technical note. National Institute of Standards and Technology; U.S. Department of Commerce: Gaithersburg, MD (2012). Available at: https://www-s.nist.gov/srmors/view_detail.cfm?srm=2686A
[22] ASTM C1365: Standard Test Method for Determination of the Proportion of Phases in Portland

Cement and Portland-Cement Clinker Using X-ray Diffraction Analysis. Annual Book of ASTM Standards. Vol. 4.01. West Conshohocken, PA: ASTM International, 2014. Available at: https://www.astm.org/Standards/C1365.htm
[23] K. Luke, F.P. Glasser, Selective dissolution of hydrated blast Furnace slag cements, Cem. Concr. Res. 17 (1987) 273-282.
[24] W. A. Gutteridge, On the dissolution of the interstitial phases in Portland cement, Cem. Concr. Res. 9 (1979) 319-324.
[25] A. Cuesta, G. Álvarez-Pinazo, M. García-Maté, I. Santacruz, M.A.G. Aranda, A.G. De la Torre, L. León-Reina, Rietveld quantitative phase analysis with molybdenum radiation, Powder Diffr. 30 (2015) 25–35.
[26] F. Fauth, I. Peral, C. Popescu, M. Knapp The new material science powder diffraction beamline at ALBA synchrotron. Powder Diffr. 28 (2013) S360−S370.
[27] G. Courbion, G. Ferey, $Na_2Ca_3Al_2F_{14}$: A new example of a structure with "independent F−"—A new method of comparison between fluorides and oxides of different formula, J. Solid State Chem. 76 (1988) 426–431.
[28] A. Kern, R.W. Cheary, A.A.Coelho, Convolution Based Profile Fitting. Diffraction Analysis of the Microstructure of Materials. Editors: Mittemeijer, E.J. & Scardi, P. Springer Series in Materials Science, 68, (2004) 17–50.
[29] W.A. Dollase, Correction of intensities for preferred orientation in powder diffractometry: application of the March model. J Appl Cryst 19 (1986) 267–272.
[30] D. Balzar, Voigt-function model in diffraction line broadening analysis. - Microstructure Analysis from Diffraction, edited by R. L. Snyder, H. J. Bunge, and J. Fiala, International Union of Crystallography (1999) 2–44.

Figure Captions

Figure 1. Particle size distribution of SRM 2686a after milling for the powder diffraction analyses.

Figure 2. Selected range (10 – 45º/ 2θ) of the Cu-Kα_1 Rietveld plots for (a) the SRM 2686a clinker, (b) the silicate enriched residue and (c) the aluminate enriched residue. The inset in figure 2b has been honestly manipulated to highlight the contributions to the overall powder pattern for the two belite polymorphs.

Figure 3. Selected range of the Rietveld plots for SRM 2686a with the diffraction peaks arising from the main phases labelled. C_3S, C_2S, C_3A and C_4AF stand for alite, belite, tricalcium aluminate and ferrite, respectively. (a) Cu-LXRPD: strictly monochromatic CuKα_1 pattern. (b) Mo-LXRPD: strictly monochromatic MoKα_1 pattern. (c) SXRPD: monochromatic synchrotron pattern.

Table 1. NIST mineralogical analysis reported for SRM 2686a from powder diffraction and electron microscopy [21]. The maximum variation allowed by ASTM C1365 test method [22] is also included.

	NIST SRM 2686a (wt%)	ASTM C1365 Maximum variation allowed (%)	Range allowed by ASTM C 1365 test method
Alite	63.35 ± 1.29	5.9	57.45-69.25
Belite	18.68 ± 1.42	3.7	14.98-22.38
Aluminate	2.46 ± 0.67	2.1	0.36-4.56
Ferrite	10.76 ± 1.44	2.5	8.26-13.26
Periclase	3.4± 0.40	0.8	2.60-4.20
Alkali Sulfates*	0.87± 0.27	0.9	0.00-1.80

* The NIST powder diffraction study reported the Reference Mass Fraction Values for alkali Sulfate Phases by XRD: aphthitalite 0.74(8) wt% and arcanite 0.27(7) wt%.

Table 2. Average RQPA results (wt%) for the silicate enriched residue (KOH-sucrose treatment) and for the aluminate enriched residue (methanol-salicylic treatment) of SRM 2686a, by using Cu-LXRPD. Numbers between parenthesis are the standard deviation values calculated from the three replicates. The results for the six analyses are given as supplementary information in Tables S2 and S3.*

	Silicate residue KOH-sucrose treatment	*Silicate residue calculated from the average composition reported for the clinker*	Aluminate residue methanol-salicylic treatment	*Aluminate residue calculated from the average composition reported for the clinker*
Alite (M_3)	78.7(1.5)	*76.7*		
β-belite	13.4(1.5)	*14.6*		
α'_H-belite	2.9(1)	*4.0*		
Cub-aluminate	-		5.3(6)	*6.9*
Ortho-aluminate	-		7.8(6)	*10.7*
Ferrite	-		69.8(1)	*57.4*
Periclase	5.0(1)	*4.6*	17.2(3)	*22.6*
Aphthitalite	-		-	*2.5*

* The expected content for every phase in the residues calculated from the average analyses of the clinker are also given (italics) for the sake of comparison.

Table 3. RQPA results, in weight percentages, obtained in this study for SRM 2686a, by using the three radiations. The RQPA results by using only β-belite are also included (in italics). NIST reported values are also included for the sake of comparison. ICSD collection codes used for RQPA are also given. Numbers between parentheses are the standard deviation of the three values for the Cu-replicates and the mathematical errors given by Rietveld method for the single analyses (Mo- and synchrotron- radiation).

	ICSD code	Cu-$_{average}$ LXRPD	*Cu-$_{average}$ LXRPD-β-belite*	Mo-LXRPD	*Mo-LXRPD-β-belite*	SXRPD	*SXRPD-β-belite*	Reported by NIST
Alite (M_3)	94742	66.0(2)	*66.3(2)*	66.9(6)	67.4(6)	65.4(3)	65.6(2)	63.35 ± 1.29
β-belite	81096	13.5(2)	*15.7(2)*	12.2(5)	14.8(5)	13.8(2)	16.2(2)	
α'$_H$-belite	81097	2.7(1)	-	3.6(4)	-	3.0(2)	-	
Total belite		*16.2*	*15.7*	*15.8*	*14.8*	*16.8*	*16.2*	*18.68 ± 1.42*
Cub-aluminate	1841	0.70(4)	*0.80(3)*	1.1(2)	1.2(2)	0.69(6)	0.69(6)	
Ortho-aluminate	100220	1.2(1)	*1.6(1)*	1.9(4)	2.4(3)	1.3(1)	1.8(1)	
Total aluminate		*1.9*	*2.4*	*3.0*	*3.6*	*1.99*	*2.49*	*2.46 ± 0.67*
Ferrite	9197	11.1(1)	*10.9(2)*	10.3(3)	10.3(3)	11.6(1)	11.6(1)	10.76 ± 1.44
Periclase	9863	4.0(1)	*3.9(1)*	3.5(1)	3.4(2)	3.65(6)	3.60(6)	3.4± 0.40
Aphthitalite	26018	0.80(3)	*0.80(3)*	0.45(7)	0.42(7)	0.57(8)	0.54(5)	*0.87± 0.27*
R_{WP} / %		*6.3**	*6.3**	*8.6*	*8.8*	*4.7*	*4.8*	

* Average of the three R_{WP} given in supplementary information.

Table 4. Final peak shape parameters employed for obtaining the RQPA results reported in Table S4, and the corresponding average in Table 3, by using the fundamental parameter approach for Cu-LXRPD patterns.

	Cu-R1 LXRPD	Cu-R2 LXRPD	Cu-R3 LXRPD
LVol FWHM Alite-M_3 /nm	171(5)	171(6)	172(5)
e0 Alite-M_3 /dimensionless	0.037(1)	0.039(1)	0.039(1)
PO coef. Alite-M_3 /dimensionless	0.947(3)	0.941(3)	0.958(3)
LVol FWHM for all belites /nm	37(2)	37(2)	38(2)
e0 for all belites /dimensionless	0.038(-)	0.038(-)	0.038(-)
LVol FWHM for all aluminates /nm	89(-)	89(-)	89(-)
e0 for all aluminates /dimensionless	-	-	-
LVol FWHM ferrite /nm	68(5)	66(5)	64(4)
e0 ferrite /dimensionless	0.175(-)	0.175(-)	0.175(-)
LVol FWHM periclase /nm	82(5)	77(5)	76(4)
e0 periclase /dimensionless	-	-	-
LVol FWHM aphthitalite /nm	50(-)	50(-)	50(-)
e0 aphthitalite /dimensionless	-	-	-

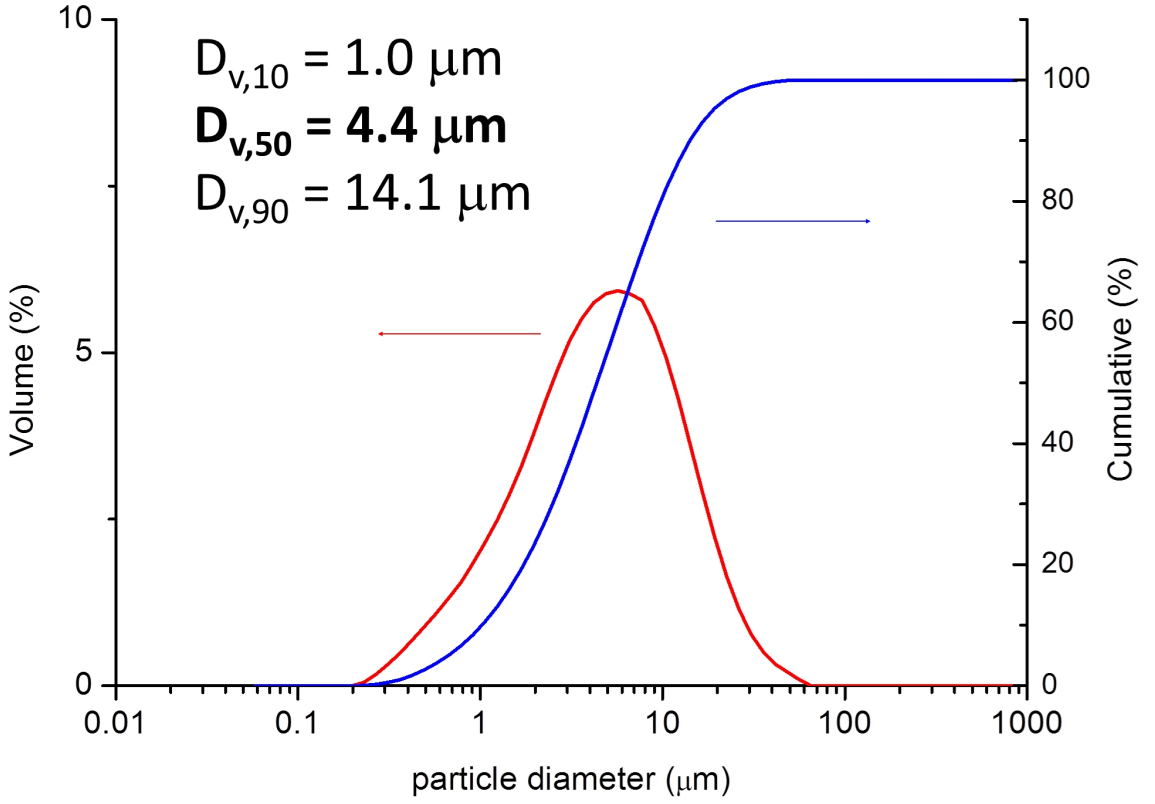
$D_{v,10}$ = 1.0 µm
$D_{v,50}$ = 4.4 µm
$D_{v,90}$ = 14.1 µm
Volume (%)
Cumulative (%)
particle diameter (µm)
0
5
10
0
20
40
60
80
100
0.01
0.1
1
10
100
1000

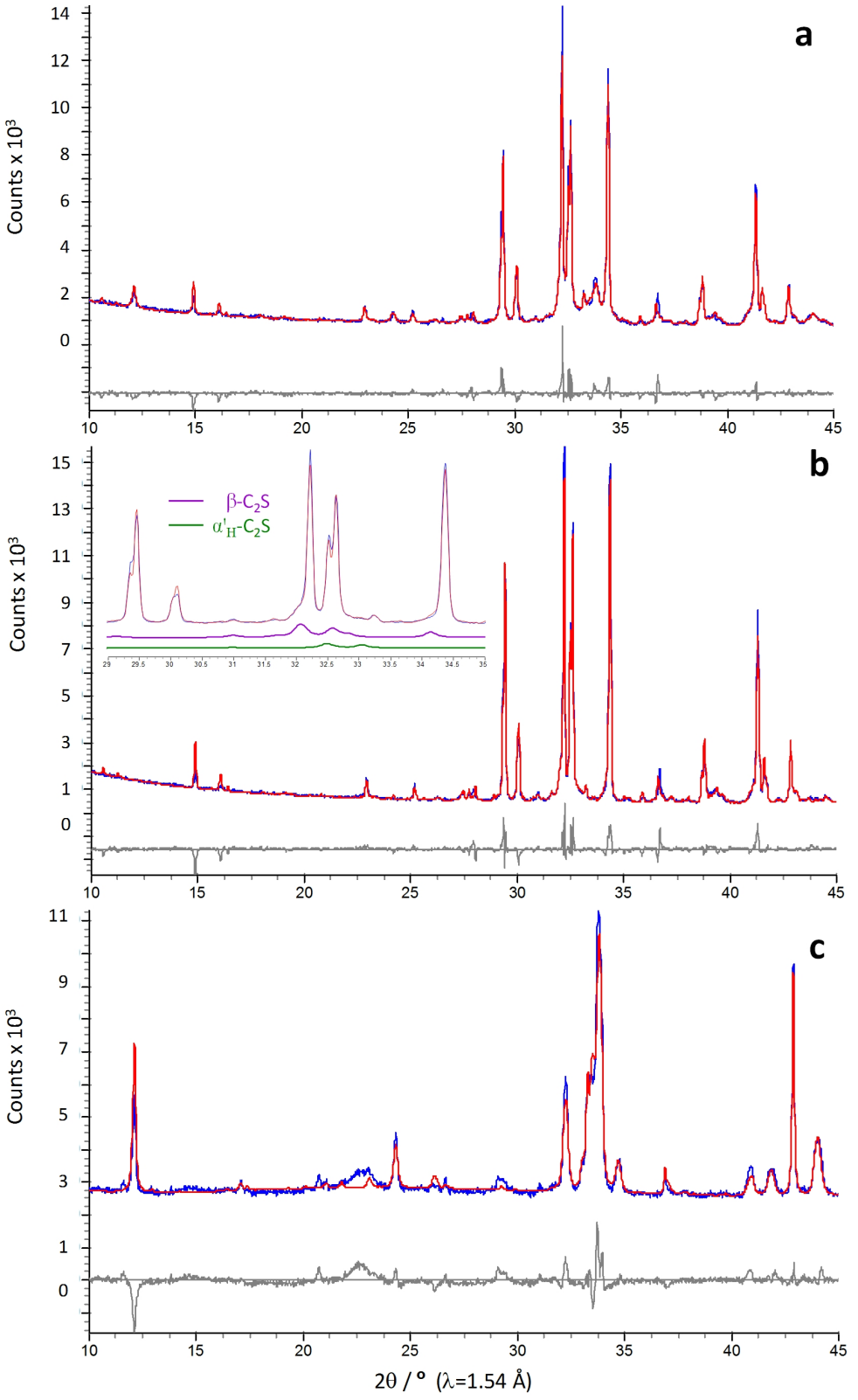
a
b
c
Counts x 10³
β-C₂S
α'H-C₂S
2θ / ° (λ=1.54 Å)

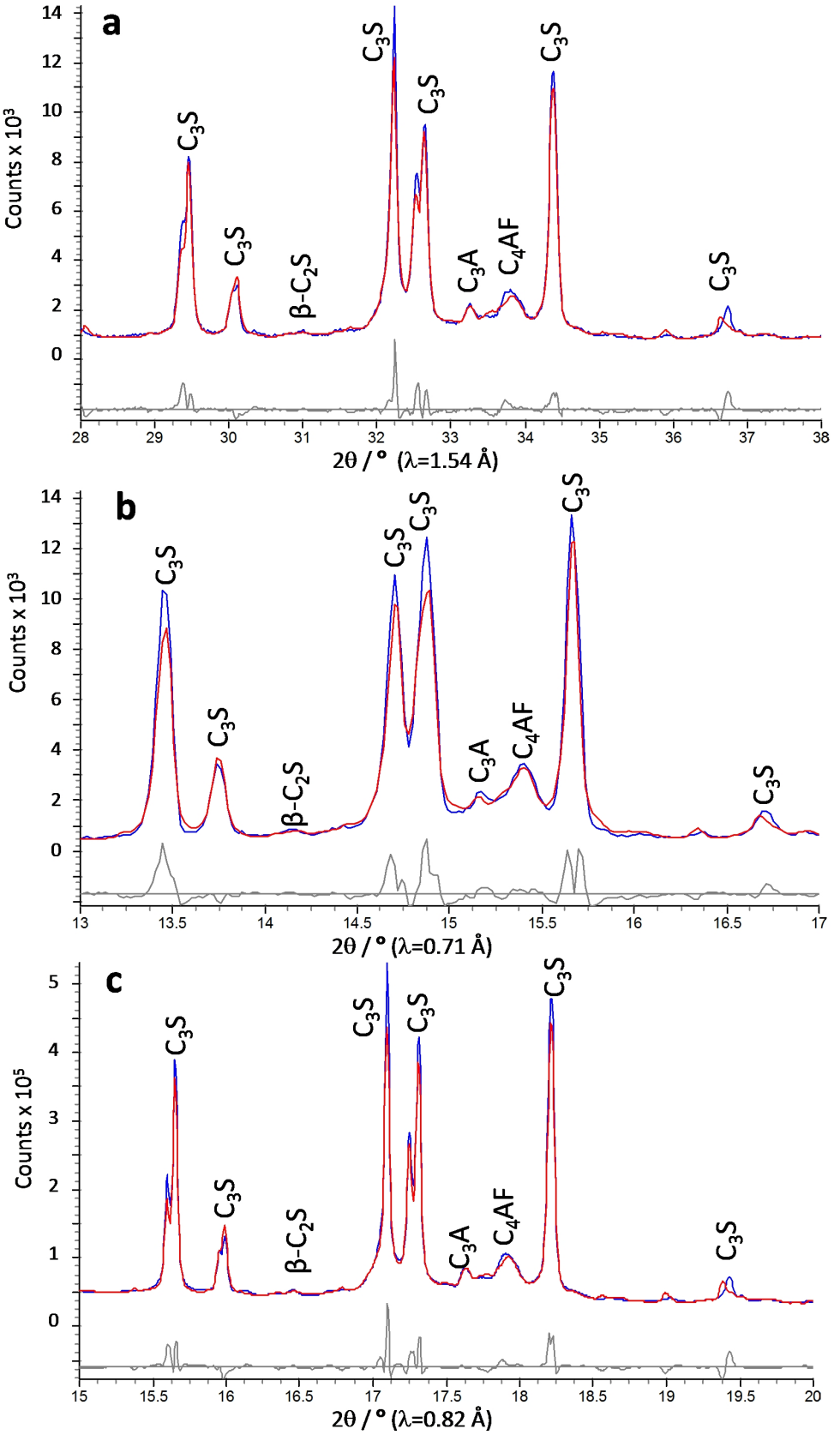
a
Counts x 10³
C3S
C3S
β-C2S
C3S
C3S
C3A
C4AF
C3S
2θ / ° (λ=1.54 Å)
b
Counts x 10³
C3S
C3S
β-C2S
C3S
C3S
C3A
C4AF
C3S
2θ / ° (λ=0.71 Å)
c
Counts x 10⁵
C3S
C3S
β-C2S
C3S
C3S
C3A
C4AF
C3S
2θ / ° (λ=0.82 Å)

Supplementary information

Rietveld Quantitative Phase Analyses of SRM 2686a: a Standard Portland Clinker

M. García-Maté[a], G. Álvarez-Pinazo[a], L. León-Reina[b], A. G. De la Torre[c], M. A. G. Aranda[c,d,*]

[a] X-Ray Data Services S.L., Edificio de Institutos Universitarios, Oficina 11C, C/ Severo Ochoa 4, Parque Tecnológico de Andalucía, 29590 Málaga, Spain.

[b] Servicios Centrales de Apoyo a la Investigación, Universidad de Málaga, 29071, Málaga, Spain.

[c] Departamento de Química Inorgánica, Universidad de Málaga, Campus Teatinos S/N. 29071, Málaga, Spain.

[d] ALBA Synchrotron, Carrer de la Llum 2-26. 08290 Cerdanyola del Vallès, Barcelona, Spain.

* email: g_aranda@uma.es or migarcia@cell.es

This supplementary information includes 4 Tables and the description of the raw powder diffraction files deposited at Zenodo.

Table S1. Rietveld refinement instrumental parameters used to collect the data for Rietveld refinements by using the fundamental parameters approach.

	Cu-LXRPD	Mo-LXRPD	SXRPD
Primary radius (mm)	240	188.5	-
Linear PSD 2θ angular range (°)	2.122	4	-
Fixed Divergent Slit angle (°)	0.5	0.1	-
Beam spill, sample length* (mm)	16	-	-
Full Axial Convolution			
Source length[$] (mm)	12	12	-
Sample length[&] (mm)	20	15	-
Receiving Slit length (mm)	12	12	-
Primary Sollers (°)	2.3	1.6	-
Secondary Sollers (°)	2.3	2.5	-
Additional Convolution, angle dependence			
Lorentzian, 1/cos(θ)	-	-	0.0001
Hat, constant	-	-	0.017
Circles, -1/tan(θ)	-	-	0.0018
Gaussian, tan(θ)	-	-	0.0468
Lorentz Polarization correction factor	27.3	20.4	90
λ (Å); Lorentzian HW[#] (mÅ)	1.5406; 0.5	0.7093; 0.27	0.825; 0.7
2θ angular range (º)	6-70	4.3-35	5-63

*Sample length for beam overflow related profile shape correction; [$]Length of the tube focus; [&] Maximum length of the irradiated sample; [#]The emission profile line is convoluted into it.

Table S2. RQPA results (wt%) for three replicates for the silicate enriched residue (KOH-sucrose treatment) of SRM 2686a, by using Cu-LXRPD.

	Cu-R1 LXRPD	Cu-R2 LXRPD	Cu-R3 LXRPD
Alite (M_3)	80.4(3)	77.9(4)	77.7(4)
β-belite	11.8(2)	14.0(4)	14.5(4)
α'_H-belite	2.8(2)	3.0(2)	2.8(2)
Periclase	5.0(1)	5.0(1)	4.9(1)
R_{WP} / %	*10.3*	*8.9*	*8.9*

Table S3. RQPA results (wt%) for three replicates for the aluminate enriched residue (methanol-salicylic) of SRM 2686a, using Cu-LXRPD.

	Cu-R1	Cu-R2	Cu-R3
Cub-aluminate	4.6(4)	5.8(7)	5.4(7)
Ortho-aluminate	8.5(5)	7.6(7)	7.3(7)
Ferrite	69.6(5)	69.8(7)	69.9(7)
Periclase	17.3(2)	16.8(3)	17.4(3)
R_{WP} / %	*3.8**	*4.6*	*4.3*

*The pattern has been analysed with an excluded region from 16.8 to 17.4 º(2θ) where a reflection due to salicylic acid was present.

Table S4. RQPA results, in weight percentages, obtained for SRM 2686a by analysing the three Cu-LXRPD replicates. NIST reported values are also included for the sake of comparison.

	Cu-R1 LXRPD	Cu-R2 LXRPD	Cu-R3 LXRPD	Reported by NIST
Alite (M_3)	65.8(4)	65.8(5)	66.2(4)	63.35 ± 1.29
β-belite	13.6(4)	13.6(5)	13.3(4)	
α'_H-belite	2.9(3)	2.7(3)	2.6(3)	
Total belite	*16.5*	*16.3*	*15.9*	*18.68 ± 1.42*
Cub-aluminate	0.7(1)	0.8(1)	0.7(1)	
Ortho-aluminate	1.0(2)	1.3(2)	1.2(2)	
Total aluminate	*1.7*	*2.1*	*1.9*	*2.46 ± 0.67*
Ferrite	11.1(2)	11.0(2)	11.2(2)	10.76 ± 1.44
Periclase	4.0(1)	4.1(1)	3.9(1)	3.4± 0.40
Aphthitalite	0.8(1)	0.8(1)	0.8(1)	
R_{WP} / %	*6.3*	*6.4*	*6.1*	

6. Description of every synchrotron powder diffraction raw data set deposited open access.

All X-ray powder diffraction raw data files underlying this article can be accessed on Zenodo at https://doi.org/10.5281/zenodo.1318500, and used under the Creative Commons Attribution license.

For the July-21st (last) version (https://doi.org/10.5281/zenodo.1318501)

Files:

Final X-ray powder diffraction data files for the quantitative analysis of SRM 2686a

Clinker_Nist_CuKalpha1_R1.xrdml
Clinker_Nist_CuKalpha1_R2.xrdml
Clinker_Nist_CuKalpha1_R3.xrdml
Clinker_Nist_MoKalpha1.raw
Clinker_Nist_Synchrotron.dat
Silicate_enriched_residue_Nist_CuKalpha1_R1.xrdml
Silicate_enriched_residue_Nist_CuKalpha1_R2.xrdml
Silicate_enriched_residue_Nist_CuKalpha1_R3.xrdml
aluminate_enriched_residue_clinkerNIST_180718_R1.xrdml
aluminate_enriched_residue_clinkerNIST_180718_R2.xrdml
aluminate_enriched_residue_clinkerNIST_180718_R3.xrdml

The May-21st version (https://doi.org/10.5281/zenodo.1318499)
This deposition contains aluminate_enriched_residue patterns with a significant presence of alite.

The February-2nd version (https://doi.org/10.5281/zenodo.1147630)
This deposition contains Cu-LXRPD patterns without any replicate.